BOLLETTINO DI GEOFISICA TEORICA ED APPLICATA VOL. 40, N. 3-4, pp. 359-367; SEP.-DEC. 1999

Further analyses towards the introduction of ocean circulation model information into geopotential solutions

N.K. PAVLIS[(1)], C.M. COX[(1)], Y.M. WANG[(1)] and F.G. LEMOINE[(2)]

[(1)] *Raytheon ITSS Corporation, Greenbelt, Maryland, USA*
[(2)] *Laboratory for Terrestrial Physics, Goddard Space Flight Center, Greenbelt, Maryland, USA*

(Received October 4, 1998; accepted August 5, 1999)

Abstract. Two representation methods for the Dynamic Ocean Topography (DOT) are compared. One uses surface spherical harmonics, the other Proudman functions, which form an ocean domain-specific orthonormal basis. The DOT implied by the temporally averaged output of the POCM_4B ocean circulation model, provided the data for the implementation and testing of the two methods. Using these data a spherical harmonic representation was developed, to degree 30, and a Proudman function decomposition employing 961 basis vectors, so that both representations involve an equal number of parameters. The input DOT field had an rms value of ±66.6 cm. The recovered rms DOT was ±66.1 cm for the spherical harmonic case, ±66.3 cm for the Proudman function case, while the rms difference between the two cases was ±4.2 cm. Although in an overall sense the two representations (with equal number of parameters) yield similar results, in the proximity of the ocean domain boundary the Proudman functions approximate the input DOT field better than the surface spherical harmonics.

1. Introduction and mathematical preliminaries

An important consideration in analyses involving the functional representation of Dynamic Ocean Topography (DOT), is the choice of a suitable set of basis functions. Surface spherical harmonics (SH) have been used for this purpose by several investigators (e.g., Marsh et al., 1990; Rapp et al., 1991). The disadvantage encountered by the loss of orthogonality of the SH over the ocean domain (which is a subset of the sphere with an irregular boundary) was recognized early on. Numerically constructed orthogonal sets of basis functions, specific to a pre-defined ocean domain (at some resolution) include the Proudman functions (PF) (Proudman, 1917), the

Corresponding author: N.K. Pavlis, Raytheon ITSS Corp., 7701 Greenbelt Road, Suite 300, Greenbelt, MD 20770, USA; phone: +1 301 441 4121; fax: +1 301 441 2432; e-mail: npavlis@magus.stx.com

© 1999 Osservatorio Geofisico Sperimentale

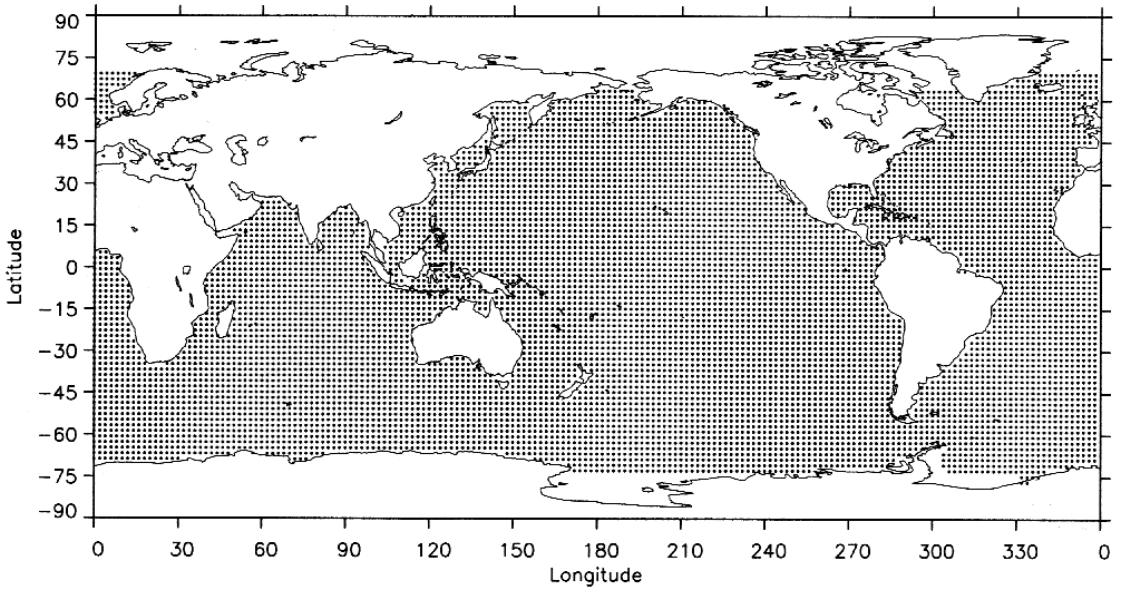

Fig. 1 - 2°×2° grid used for the Proudman function development.

"Height" functions (HF) introduced by Rao et al. (1987), and the orthonormal functions (ON) introduced by Hwang (1991; 1995) which are derived from SH. Rapp et al. (1996) recommended the use of SH for DOT representation, followed by transformation to the ON basis, which enables spectral analysis referring strictly to the ocean domain. Sanchez et al. (1997) implemented the HF representation and compared it with SH. PF were used recently in the tidal analysis performed by Sanchez and Pavlis (1995). Colombo (1984) suggested using PF for DOT representation. This has never been attempted up to now. This paper presents preliminary results from the use of PF for DOT representation, and a comparison with corresponding results based on the use of SH.

The detailed mathematical formulation underlying the development of the PF basis can be found in (Sanchez et al., 1985) and will not be repeated here. Partition of the transport field into solenoidal and irrotational components and the application of the divergence operator yields the eigenvalue problem from which the velocity potential eigenvectors (Φ_γ) are derived:

$$\nabla \cdot h \nabla \Phi_\gamma = -\lambda_\gamma \Phi_\gamma \tag{1}$$

The impermeability of the coast provides the associated boundary conditions:

$$h \cdot (\partial \ \Phi_\gamma / \partial n) = 0 \tag{2}$$

where h denotes the depth of the fluid and n is the direction normal to the boundary. The subscript γ

has a range determined by the number of degrees of freedom allowed by the system. The numerical solution of the eigensystem (1) was obtained by means of finite differences expressed in spherical coordinates. A 2° equiangular grid was used, extending from 69.25° N to 76.75° S latitude (Fig. 1). The resulting system has 8608 degrees of freedom. Enclosed basins (Mediterranean, Hudson Bay, etc.) are excluded; these require individual analyses with grids of much finer resolution (Sanchez et al., 1992), while this study is focusing on the estimation over open ocean areas. The Arctic ocean is also excluded in this grid. The resulting unitless eigenvectors (Φ_γ) are normalized, so that:

$$\frac{1}{A}\iint_{\text{basin}} \Phi_\gamma \Phi_\beta dA = \delta_{\gamma\beta} \tag{3}$$

where A is the total area of the basin and $\delta_{\gamma\beta}$ is the Kronecker delta. The PF set (Φ_γ) used here is the same as the one used in (Sanchez and Pavlis, 1995). Examples of the spatial structure of Φ_γ can be found in (ibid., Fig. 3). The spatial variability of Φ_γ increases with increasing wave number γ; however, over enclosed oceanic areas or areas close to the boundary, even the low wave number eigenvectors exhibit large geographical variations (e.g., Kamchatka peninsula, Patagonian shelf).

2. DOT analysis with Proudman functions and surface spherical harmonics

The DOT implied by the POCM_4B circulation model of Semtner and Chervin (cf. Stammer et al., 1996) provided the test data for the implementation of the SH and PF representation methods. The DOT values used ($\zeta(\varphi,\lambda)$), are the temporally averaged output of POCM_4B over the years 1993 and 1994. No spatial averaging was performed.

2.1. Proudman function analysis

The values of the first 1200 PF eigenvectors were interpolated at the nodes of the POCM grid. Because the POCM and the PF grids discretized the ocean independently, and in a slightly different fashion, there are 16 938 POCM points (covering about 2.7% of the Earth's area), where Φ_γ cannot be interpolated. There are also a few nodes of the PF grid, where POCM is undefined; these cover (approximately) latitudes 64.85° to 69.25° N, and longitudes -30° to +15°. There is a rather good overall "alignment" between the POCM and the PF grids. The 299 256 points, where both POCM and Φ_γ are defined, is what we consider hereon to be our "ocean domain" (OD). The OD covers 65.4% of the Earth's area, where the POCM_4B DOT ranges from -210.4 to 133.1 cm, with area weighted mean and rms values of 0.5 cm and ±66.6 cm, respectively. Using these data, we formed normal equations for 1200 PF coefficients, P_k , based on the linear mathematical model:

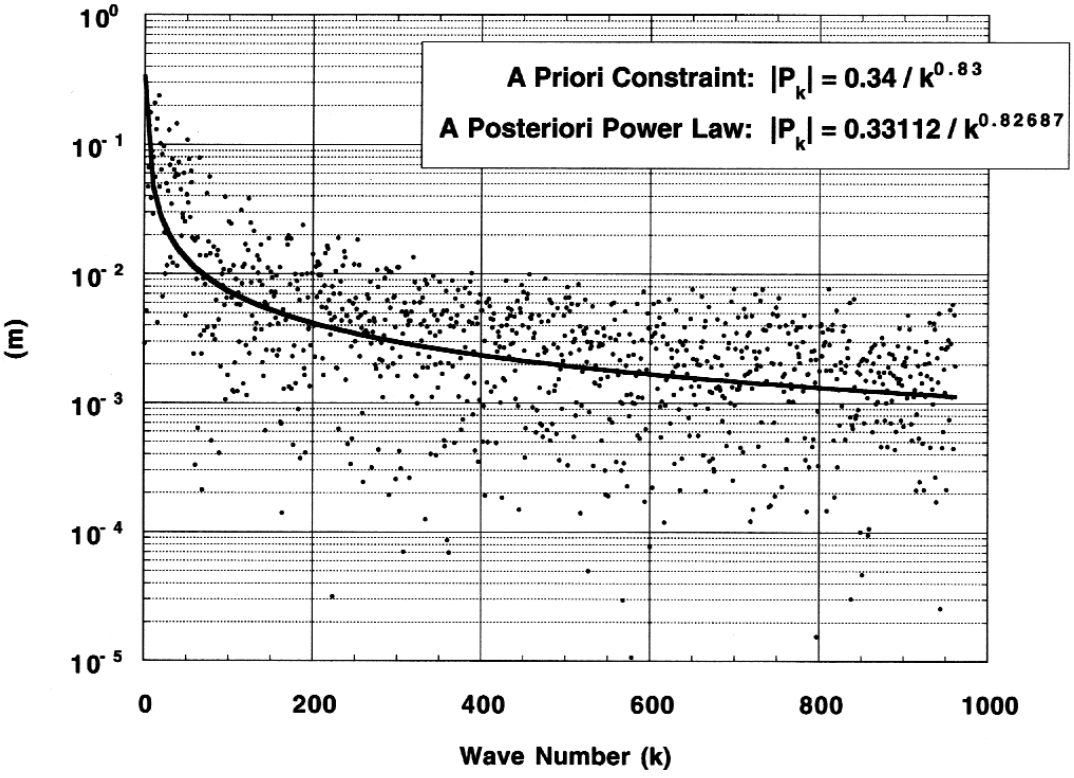

Fig. 2 - Estimated Proudman function coefficient magnitude ($|P_k|$).

$$\zeta(\varphi,\lambda) = \sum_{k=1}^{1200} P_k \cdot \Phi_k(\varphi,\lambda) \tag{4}$$

Each $\zeta(\varphi,\lambda)$ value received a weight $w = \cos^2(\varphi)/0.1^2$ m^{-2}.

To enable comparisons with SH representations employing an equal number of parameters, the PF least squares solution was restricted to the first 961 eigenvectors. Their coefficients were estimated using the a priori constraint $|P_k| = 0.34/k^{0.83}$ m in the inversion of the normal equations. This power law was derived empirically from the data. Fig. 2 shows the magnitude spectrum ($|P_k|$) of the recovered PF coefficients. Over the OD, the DOT reconstructed from these coefficients has an area weighted rms value of ±66.3 cm. The area weighted rms residual misfit was ±6.1 cm.

2.2. Spherical harmonic analysis

Our analysis closely followed the procedures used by Rapp et al. (1996). Over the OD, the data and their weights were identical to the PF case. Outside the OD (areas that are mostly but not exclusively land), we used zero "fill-in" values, over $-60° \le \varphi \le 75°$, weighted by $w = \cos^2(\varphi)/0.2^2$ m^{-2}. Thus a 4:1 weight ratio between actual and "fill-in" data at a given latitude was

Table 1 - Classification of residuals of fit, recoverd DOT signal and signal differences as a function of minimum distance *D* from the boundary, for the SH and PF solutions.

Range of *D* (km)	% of Total Data Area	Spherical Harmonic (SH) (*Nmax*=30)		Proudman function (PF) (961 eigenvectors)		SH-PF
		RMS residual (cm)	RMS signal (cm)	RMS residual (cm)	RMS signal (cm)	RMS signal (cm)
0 - 50	0.2	12.7	62.6	9.7	69.0	13.4
50 - 100	1.0	12.7	64.9	11.6	70.1	12.6
100 - 150	1.8	11.7	63.8	9.7	68.3	11.1
150 - 200	2.4	10.4	68.8	7.4	72.1	9.4
200 - 250	2.6	9.3	69.1	6.5	71.4	7.6
250 - 500	12.0	7.9	74.0	7.0	74.2	4.8
500 - 1000	19.0	6.4	78.9	6.6	78.7	4.0
1000 - 1500	16.6	5.5	75.1	5.9	75.0	3.1
1500 - 2000	13.7	5.3	64.6	5.4	64.5	2.6
2000 - 2500	10.0	5.7	50.7	5.9	50.8	2.5
2500 - 3000	6.8	4.6	41.5	5.0	41.5	2.5
3000 - 3500	4.6	2.9	42.5	4.0	42.0	2.6
3500 - 4000	3.4	2.8	45.2	4.3	45.4	2.8
4000 - 5000	5.2	2.5	47.0	4.2	46.8	2.5
5000 - 9999	0.8	2.1	47.6	3.6	47.6	2.0

maintained. The SH coefficients to *Nmax* = 30 were obtained from a least squares solution, with the a priori constraint $|SH_n| = 0.30775/n^{1.4243}$, for the rms SH coefficient of degree *n*. Over the OD region the area weighted rms residual misfit and reconstructed DOT signal from this SH fit were ±6.2 cm and ±66.1 cm respectively.

3. Comparison of the two representation methods

3.1. Signal recovery and residual misfits

The area weighted rms difference of the DOT fields reconstructed from the two representation methods was ±4.2 cm, indicating a good overall agreement between the two different representations, when an equal number of parameters are used in each method. However, plots of the residual misfits (not shown here) from the respective adjustments, indicated that significant differences exist in the geographical distribution of these residuals for the two different methods. Specifically, the PF approach appeared to fit the input data better, close to the OD boundary, compared to the SH approach. By contrast, over certain open ocean areas (e.g., west-central Pacific), the SH approach appeared to fit the data better. To quantify these visual observations we computed the rms residual misfit and rms recovered signal from each method, as a function of minimum distance (*D*) from the OD boundary. Table 1 summarizes these results, for a selection of ranges of *D*. From Table 1 it is obvious that the

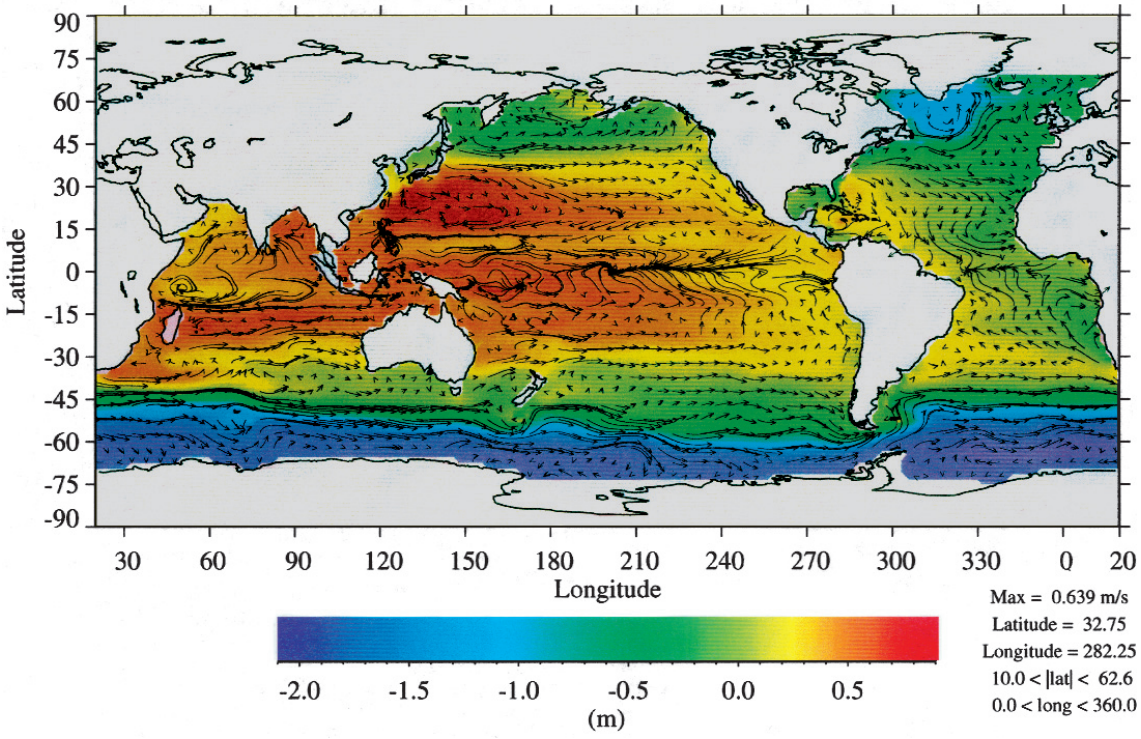

Fig. 3 - DOT and geostrophic flow vectors from the Proudman function fit of POCM_4B using 961 eigenvectors.

largest differences in the two recovered DOT fields are indeed occurring within ~250 km from the OD boundary. In this region, the PF representation recovers a DOT signal of significantly higher power than that recovered from SH. The PF-recovered signal is in closer agreement with the input data over this region, as reflected by the smaller residuals obtained from the PF fit, compared to those from the SH fit. For $D > 3000$ km or so, the residuals from the SH fit are smaller than those from the PF by about 30%.

A possible explanation for the observed behavior may be the following. Surface SH functions vary over the sphere in a regular manner dictated by their degree and order, with no regard to proximity to the OD boundary. Proudman functions exhibit a different behavior, and, judging from plots shown in Sanchez and Pavlis (1995), Fig. 3, tend to be smoother away from the boundary. This could result in PF being capable of modeling short wavelength data signals close to the boundary better than SH, and vice versa away from the boundary. In practical applications using PF, this implies that if one wants to maintain the modeling capability of SH (up to some *Nmax*) over open ocean areas, it may be appropriate to extend the PF set vector beyond $(Nmax + 1)^2$ elements. PF solutions using more than 961 vectors will be made in the future, to investigate this effect.

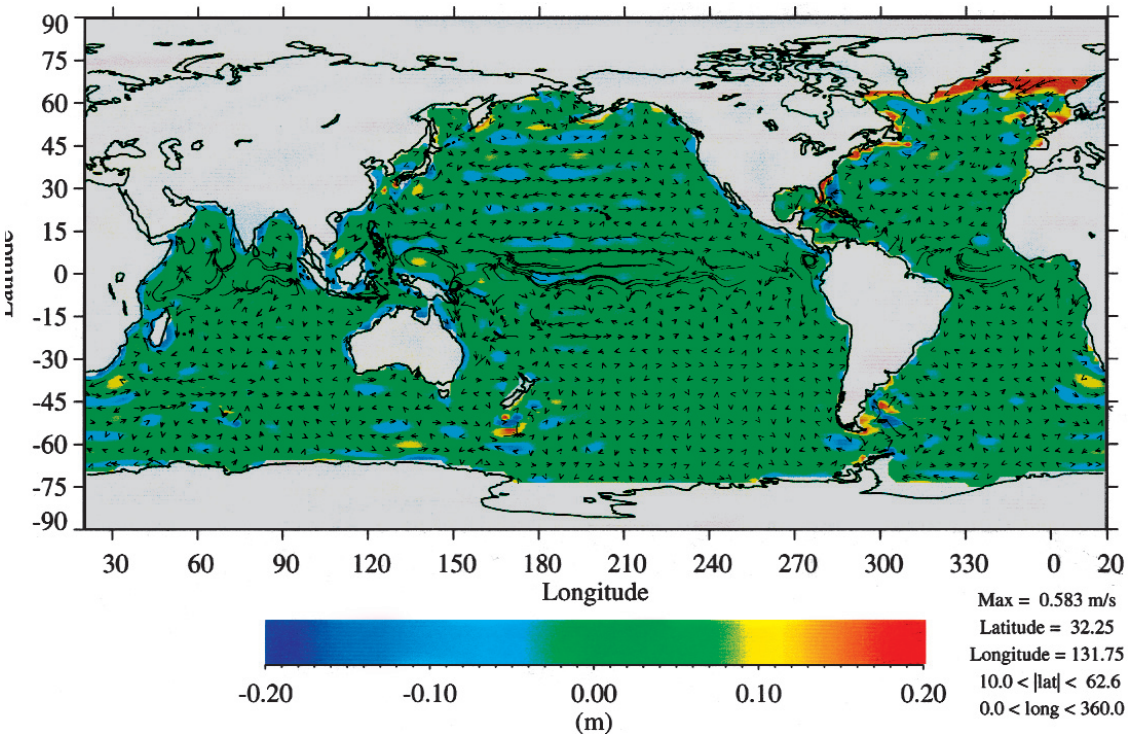

Fig. 4 - DOT and geostrophic flow vector differences: SH (*Nmax*=30) minus Proudman function fit using 961 eigenvectors.

3.2. Geostrophic flow velocity calculations

In the SH approach, the components of the geostrophic velocity vector were computed from the recovered coefficients, using analytical expressions (see e.g., Engelis, 1985, Eqs. 21-23). Unfortunately, corresponding expressions are not available (to our knowledge) for the PF case. In this case, the fundamental equations defining the *(u,v)* components (ibid., Eqs. 17, 18) were used, and the derivatives were approximated by first differences. A 15'×15' grid of DOT was constructed from the recovered PF coefficients, and the *(u,v)* components were then computed at the centers of 30'×30' cells, provided all four surrounding nodes had defined PF values. Fig. 3 shows the recovered DOT and geostrophic flow field using 961 PF vectors, and Fig. 4 the difference of the DOT and flow fields between the SH (*Nmax* = 30) and the PF (961 vector) cases. Large differences in the DOT (Fig. 4) between Greenland and Scandinavia are related to a certain lack of overlap between the POCM_4B and PF grids. Apart from this area, large differences are seen in some coastal areas e.g., around Indonesia, northern Australia and the east African coast and Madagascar. Areas close to the boundary, characterized by steep DOT slopes (e.g., Gulf Stream, Kuroshio, Patagonia), also exhibit large differences between the SH and PF approaches. The rms total geostrophic velocity magnitude, $V = (u^2 + v^2)^{1/2}$, was ±3.99 cm/s (SH), ±4.27 cm/s (PF), and ±3.33 cm/s for the difference (SH-PF). The maximum velocity magnitudes

were: 37.83 cm/s (SH), 63.87 cm/s (PF), and 58.30 cm/s (SH-PF). PF with 961 vectors recover a signal with slightly higher overall power, than SH (*Nmax* = 30), and this is reflected in both the recovered DOT and the geostrophic velocity fields. Although the flow patterns recovered by the two approaches are in very good general agreement, differences exist (especially in the N-S component *v*), which require further study and clarification. The computational difference (analytic for SH versus numerical for PF) may also play a role here.

4. Summary and conclusions

Proudman functions were used for the first time to represent DOT. Corresponding spherical harmonic analysis was made using an equal number of parameterization coefficients, and the PF and SH results were compared. Based on the preliminary results obtained, we draw the following conclusions:

1. PF and SH results using an equal number of parameters agree quite well in overall spectral content, with the PF approach capturing slightly more power, than the SH one;
2. PF appear to be better suited for the representation of high frequency signals close to the data boundary, but are somewhat smoother away from it;
3. some differences are observed in the recovered geostrophic velocity fields between the PF and SH cases. Additional study is needed to clarify this result.

A significant advantage of PF over SH is that the former require no artificial "fill-in" values over areas where DOT is undefined. Over the ON representation introduced by Hwang (1991), PF have the advantage that they can extend the expansion of DOT to much higher wave numbers than the ON functions. The current PF set has a total of 8608 associated eigenvectors. An ON basis matching that number of basis vectors would correspond to harmonic degree ≈ 91, and such a high resolution ON set has never been developed for any realistic ocean domain definition.

For applications that require the spectral comparison of the DOT signal and the geoid undulation error, strictly over the ocean domain, we need to investigate techniques to map the latter on the Proudman function space. If such mapping can be established, the Proudman functions could offer a rather attractive alternative to the use of either SH or ON functions, for DOT representation and estimation. The development of such a mapping will be the major focus of future work within this investigation.

Acknowledgments. We thank Robin Tokmakian (Naval Postgraduate School) who provided the POCM_4B Dynamic Ocean Topography output used in this study, and Braulio V. Sanchez (NASA Goddard Space Flight Center) who gave us permission to use the Proudman function set that he and his colleagues developed some years ago. This paper was originally presented at the second joint meeting of the International Gravity Commission and the International Geoid Commission held in Trieste, Italy, September 7-12, 1998.

References

Colombo O. L.; 1984: *Altimetry, Orbits and Tides.* NASA Technical Memorandum 86180, Greenbelt, Maryland, USA.

Engelis T.; 1985: *Global Circulation from SEASAT Altimeter Data.* Marine Geodesy, **9**, 45-69.

Hwang C.; 1991: *Orthogonal Functions Over the Oceans and Applications to the Determination of Orbit Error, Geoid and Sea Surface Topography from Satellite Altimetry.* Rep. 414, Dep. of Geod. Sci. and Surv., Ohio State Univ., Columbus, Ohio, USA.

Hwang C.; 1995: *Orthonormal Function Approach for Geosat Determination of Sea Surface Topography.* Marine Geodesy, **18**, 245-271.

Marsh J. G., Koblinsky C. J., Lerch F., Klosko S. M., Robbins J. W., Williamson R. G. and Patel G. B.; 1990: *Dynamic sea surface topography, gravity, and improved orbit accuracies from the direct evaluation of SEASAT altimeter data*. J. Geophys. Res., **95**, 13 129-13 150.

Proudman J.; 1917: *On the dynamical equations of the tides, I, II, III.* Proc. London Math. Soc., **18**, 1-68.

Rao D. B., Steenrod S. D. and Sanchez B. V.; 1987: *A Method of Calculating the Total Flow From a Given Sea Surface Topography.* NASA Technical Memorandum 87799, Greenbelt, Maryland, USA.

Rapp R. H., Wang Y. M. and Pavlis N. K.; 1991: *The Ohio State 1991 geopotential and sea surface topography harmonic coefficient models.* Rep. 410, Dep. of Geod. Sci. and Surv., Ohio State Univ., Columbus, Ohio, USA.

Rapp R. H., Zhang C. and Yi Y.; 1996: *Analysis of dynamic ocean topography using TOPEX data and orthonormal functions*. J. Geophys. Res., **101**, 22 583-22 598.

Sanchez B. V., Rao D. B. and Wolfson P. G.; 1985: *Objective Analysis for Tides in a Closed Basin.* Marine Geodesy, **9**, 71-91.

Sanchez B. V., Ray R. D. and Cartwright D. E.; 1992: *A Proudman-function expansion of the M2 tide in the Mediterranean Sea from satellite altimetry and coastal gauges.* Oceanologica Acta, **15**, 325-337.

Sanchez B. V. and Pavlis N. K.; 1995: *Estimation of main tidal constituents from TOPEX altimetry using a Proudman function expansion.* J. Geophys. Res., **100**, 25 229-25 248.

Sanchez B. V., Cunningham W. J. and Pavlis N. K.; 1997: *The calculation of the dynamic sea surface topography and the associated flow field from altimetry data: a characteristic function method*. J. Phys. Oceanogr., **27**, 1371-1385.

Stammer D., Tokmakian R., Semtner A. and Wunsch C.; 1996: *How well does a 1/4° global circulation model simulate large-scale oceanic observations?* J. Geophys. Res., **101**, 25 779-25 812.